JOURNAL OF GEOPHYSICAL RESEARCH, VOL. 105, NO. B12, PAGES 28,461–28,475, DECEMBER 10, 2000

First-order reversal curve diagrams: A new tool for characterizing the magnetic properties of natural samples

Andrew P. Roberts

School of Ocean and Earth Science, University of Southampton, Southampton Oceanography Centre Southampton, England, United Kingdom

Christopher R. Pike and Kenneth L. Verosub

Department of Geology, University of California, Davis

Abstract. Paleomagnetic and environmental magnetic studies are commonly conducted on samples containing mixtures of magnetic minerals and/or grain sizes. Major hysteresis loops are routinely used to provide information about variations in magnetic mineralogy and grain size. Standard hysteresis parameters, however, provide a measure of the bulk magnetic properties, rather than enabling discrimination between the magnetic components that contribute to the magnetization of a sample. By contrast, first-order reversal curve (FORC) diagrams, which we describe here, can be used to identify and discriminate between the different components in a mixed magnetic mineral assemblage. We use magnetization data from a class of partial hysteresis curves known as first-order reversal curves (FORCs) and transform the data into contour plots (FORC diagrams) of a two-dimensional distribution function. The FORC distribution provides information about particle switching fields and local interaction fields for the assemblage of magnetic particles within a sample. Superparamagnetic, single-domain, and multidomain grains, as well as magnetostatic interactions, all produce characteristic and distinct manifestations on a FORC diagram. Our results indicate that FORC diagrams can be used to characterize a wide range of natural samples and that they provide more detailed information about the magnetic particles in a sample than standard interpretational schemes which employ hysteresis data. It will be necessary to further develop the technique to enable a more quantitative interpretation of magnetic assemblages; however, even qualitative interpretation of FORC diagrams removes many of the ambiguities that are inherent to hysteresis data.

1. Introduction

Magnetic hysteresis loops have been widely used in rock magnetic and environmental magnetic studies since the commercial development of highly sensitive alternating gradient magnetometers [*Flanders*, 1990]. The standard hysteresis parameters M_r, M_s, H_c, and H_{cr} (where M_r is the saturation remanence, M_s is the saturation magnetization, H_c is the coercive force, and H_{cr} is the coercivity of remanence) are often the only hysteresis parameters used to characterize geological samples. These parameters represent the composite magnetic response of all particles within a sample, and, therefore, provide a measure of the bulk magnetic properties of the sample. The scheme of *Day et al.* [1977], which is based on the M_r/M_s and H_{cr}/H_c ratios, has become a standard tool for discriminating relative variations in domain state (and hence magnetic grain size) for materials containing titanomagnetite and magnetite. However, interpretation of these hysteresis parameters can be ambiguous. For example, "pseudo-single domain" M_r/M_s values of 0.2-0.3 and H_{cr}/H_c values of 2.5-3.0 are typical of many sedimentary environments [e.g., *Tauxe*, 1993; *Tarduno*, 1994; *Roberts et al.*, 1995a; *Lehman et al.*, 1996; *Stoner et al.*, 1996]. These values can arise in several ways, including samples with: a narrow grain size distribution in the pseudo-single domain (PSD) size range; a wide grain size distribution which includes both superparamagnetic (SP) and single domain (SD) grain sizes (where the SP grains reduce the overall remanence and coercivity to produce an average "PSD" value); or mixtures of SD and MD grains (where the MD grains reduce the overall remanence and coercivity of the assemblage to produce an average PSD value).

Data from samples with variable mixtures of magnetic particles tend to fall on distinct trends in plots of M_r/M_s versus H_{cr}/H_c. Such trends have been widely exploited to identify mixing lines between different magnetic components in a sample [e.g., *Parry*, 1982; *Jackson*, 1990; *McCabe and Channell*, 1994; *Channell and McCabe*, 1994; *Tauxe et al.*, 1996]. However, even in such cases, use of the standard hysteresis parameters does not provide a detailed understanding of the individual magnetic components in a sample.

Magnetostatic interactions can also produce ambiguities when interpreting hysteresis data. Magnetic interactions among particles can significantly reduce M_r/M_s [e.g., *Cisowski*, 1981; *Dankers*, 1981; *Dunlop*, 1981] and can increase H_{cr}/H_c values [*Corradi and Wohlfarth*, 1978; *Sprowl*, 1990]. Clearly, there is a need for methods that enable more detailed characterization than can be provided by these "bulk" hysteresis parameters.

In this paper, we describe a new tool (FORC diagrams) that can be used to identify the presence or absence of magnetostatic interactions and to identify the contributions of SP, SD, PSD and MD grains to the magnetization of a sample. We also

Paper number 2000JB900326.
0148-0227/00/2000JB900326$09.00

demonstrate that FORC diagrams can enable more detailed characterization of individual magnetic components, within a single sample, than can be achieved with existing techniques.

2. FORC Diagrams

A FORC diagram is calculated from a class of partial hysteresis curves known as first-order reversal curves or FORCs [see *Mayergoyz*, 1986]. As shown in Figure 1a, measurement of a FORC begins by saturating a sample with a large positive applied field. The field is decreased to a reversal field H_a, and the FORC is defined as the magnetization curve that results when the applied field is increased from H_a back to saturation. This measurement procedure is repeated for different values of H_a to obtain a suite of FORCs (Figure 1b). The magnetization at the applied field H_b on the FORC with

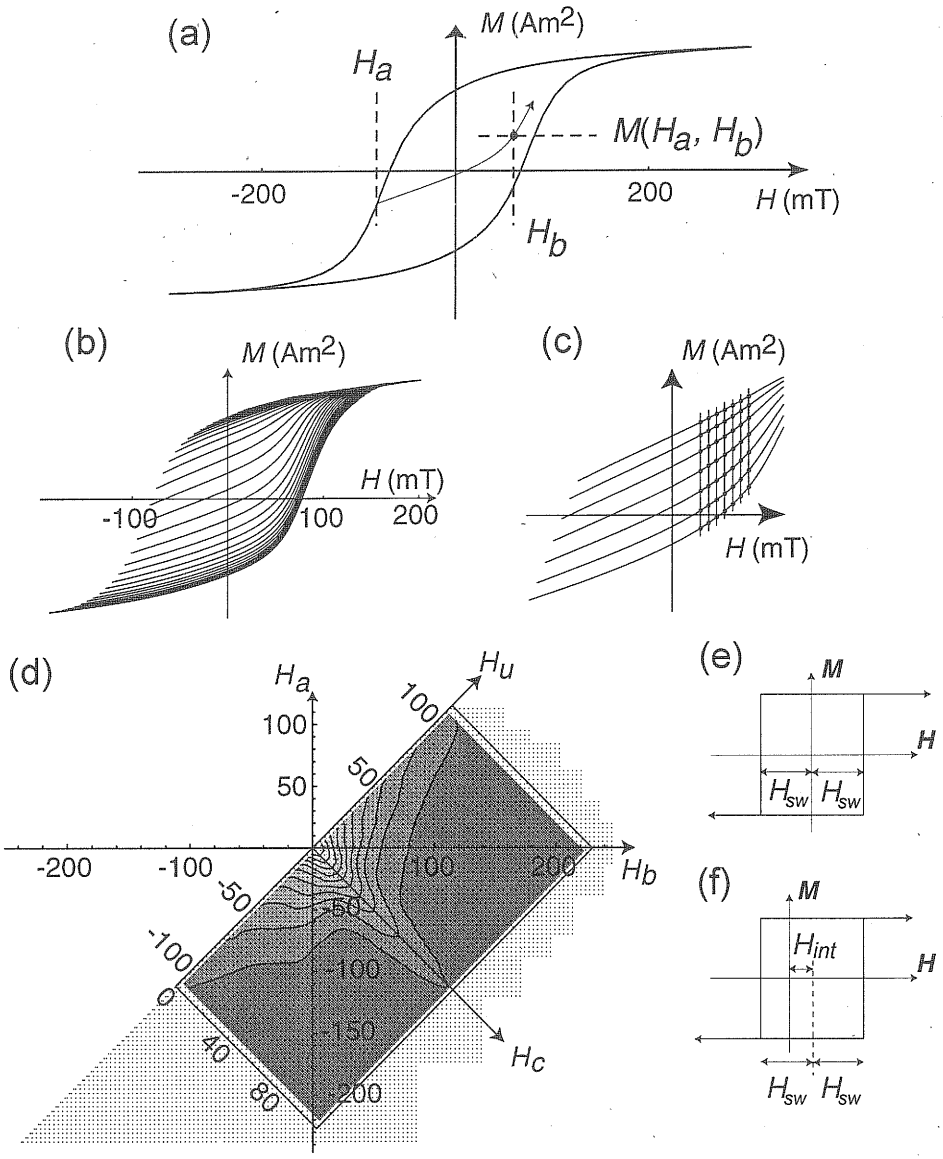

Figure 1. Illustration of construction and interpretation of FORC diagrams. (a) Example of a major hysteresis loop with reversal point at H_a. The first-order reversal curve (FORC) is the curve that starts at H_a and proceeds back to positive saturation. The magnetization at any point H_b along the FORC is represented by $M(H_a, H_b)$. (b) A set of 33 FORCs for a typical floppy disk sample. (c) A subset of seven consecutive FORCs from Figure 1b. The circled points represent a 7 x 7 array ($SF = 3$) of evenly spaced data points in H_a and H_b. (d) A $\{H_a, H_b\}$ plot, with the $\{H_c, H_b\}$ coordinate axes superimposed. The leftmost point on each row of data points represents the reversal point (H_a) for each FORC and subsequent points represent H_b values. The grid points illustrate the data density used to calculate the FORC distribution with a set of 99 FORCs; a FORC distribution is superimposed on the grid for the purpose of illustration ($SF = 4$). The sample is a MD magnetite-bearing sediment from the northeast Pacific Ocean (sample ODP-887B-2H-6-20). (e) Hysteresis loop for an isolated SD particle, with the applied field acting along the easy axis of magnetization. In this case, H_{sw} is the switching field for the particle. (f) Hysteresis loop for the same SD particle with a constant local interaction field acting parallel to the applied field and the magnetic easy axis of the grain. In this case, H_{int} is a constant local interaction field.

reversal point H_a is denoted by $M(H_a, H_b)$, where $H_b \geq H_a$ (Figure 1a). Data from consecutive measurement points on consecutive reversal curves (Figure 1c; see below) are used to determine the FORC distribution, which is defined as the mixed second derivative:

$$\rho(H_a, H_b) \equiv -\frac{\partial^2 M(H_a, H_b)}{\partial H_a \partial H_b}, \quad (1)$$

where $\rho(H_a, H_b)$ is well defined for $H_b > H_a$.

When a FORC distribution is plotted, it is convenient to change coordinates from $\{H_a, H_b\}$ to $\{H_u = (H_a + H_b)/2, H_c = (H_b - H_a)/2\}$ (Figure 1d). A FORC diagram is a contour plot of a FORC distribution with H_u and H_c on the vertical and horizontal axes, respectively (Figures 2-10). $H_b > H_a$, therefore $H_c > 0$, and a FORC diagram is confined to the right-hand half plane. An isolated SD particle, with an applied field acting along the easy axis of magnetization, and with a switching field H_{sw} (Figure 1e), would contribute to a FORC distribution at $\{H_c = H_{sw}, H_u = 0\}$. The same SD particle, when placed in a constant local interaction field H_{int} that acts parallel to the applied field (Figure 1f), would contribute to a FORC distribution at $\{H_c = H_{sw}, H_u = H_{int}\}$. Thus, as a general approximation, a FORC diagram for an assemblage of SD grains describes the distribution of particle switching fields (i.e., coercivities) and local interaction fields.

To evaluate a FORC diagram, boundary values of the desired diagram are selected in the H_u, H_c plane. The reversal field (H_a) of the first FORC is set near the H_a coordinate value at the upper left-hand corner of the desired diagram and the reversal field of the last FORC is set near the H_a coordinate at the lower right-hand corner of the FORC diagram (Figure 1d). Then, a set of FORCs is measured with evenly spaced reversal fields between, and including, the end points described above; on each individual FORC, the magnetization is measured with the same field spacing. The averaging time spent at each data point must be the same. The result is a set of measured FORCs such as those shown in Figure 1b. In choosing the number of FORCs to be measured, there is a trade-off between the resolution of the FORC diagram and data acquisition time. We have found that measuring 99 curves yields a reasonable resolution in an acquisition time of <2 hours. All of the measurements presented in this paper were performed with a Princeton Measurements Corporation Micromag alternating gradient magnetometer, with maximum field capability of 1.4 T. In principle, any vibrating sample magnetometer or alternating gradient magnetometer could be used for such measurements, although, because of the large number of measurements required, speed of measurement is an important consideration.

The field increments used to measure a set of FORCs are equal, therefore in the $\{H_a, H_b\}$ coordinate system, the data points will plot on an evenly spaced grid (Figure 1d). To evaluate the FORC distribution $\rho(H_a, H_b)$ at a point P on this grid, we use a local, square grid of data points with P at the center. The number of points on the local grid is $(2SF + 1)^2$, where SF is a "smoothing factor" that can be set between 2 for well-behaved samples and 7 for samples with low signal/noise ratios. The local grid will consist of consecutive data points from consecutive reversal curves, as shown in Figure 1c. For $SF = 3$, smoothing is performed across a 7 x 7 array of data points (Figure 1c). The magnetization at these data points is fitted with a polynomial surface of the form: $a_1 + a_2H_a + a_3H_a^2 + a_4H_b + a_5H_b^2 + a_6H_aH_b$. The value of $-a_6$ represents $\rho(H_a, H_b)$ at P. To construct a FORC diagram, $\rho(H_a, H_b)$ is evaluated at all grid points within the boundaries of the diagram, and a contour plot is constructed from these values (see Figure 1d).

Taking the second derivative in equation (1) magnifies the noise that is inevitably present in the magnetization measurements. Therefore FORC diagrams produced with $SF = 1$ (Figure 2a) can contain a large amount of noise. This noise can be removed by increasing the size of the local square grid on which the polynomial fit is performed (i.e., by increasing SF),

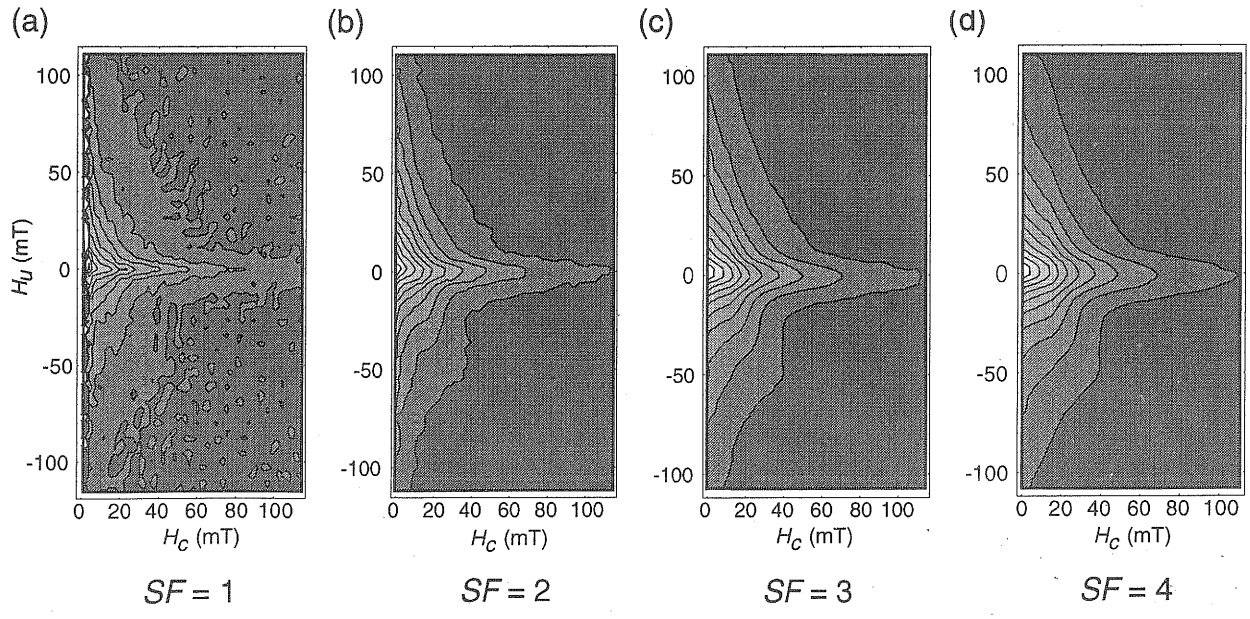

Figure 2. Illustration of the effects of smoothing on FORC diagrams. (a)-(d) FORC diagrams for sample ODP-887B-2H-6-20 (northeast Pacific Ocean) for SF values of 1, 2, 3, and 4, respectively.

as shown in Figures 2a-2d. It is clear that, for this particular sample (Figure 2), noise is effectively removed at $SF = 3$. However, the cost of increasing SF is that the features of the FORC distribution are increasingly smoothed, the resolution of the FORC diagram is reduced and fine-scale features can disappear. In practice, one uses the smallest value of SF possible, while keeping noise on a FORC diagram to acceptable levels. For most of the natural samples discussed in this paper, we use $SF = 3$.

3. Comparison With Preisach Diagrams

There are obvious similarities between a FORC diagram and a *Preisach* [1935] diagram. Both are contour plots of a two-dimensional distribution function in a half plane and both diagrams use the same notation for the coordinate axes, i.e., H_u and H_c. In the case of SD particle systems, the FORC and Preisach distributions will both approximately correspond to the distribution of particle switching fields and local interaction fields. Furthermore, a Preisach distribution is sometimes obtained using the same measurement procedure that is used to determine a FORC distribution. However, the resulting distribution must be symmetrized to be considered a legitimate Preisach distribution. In some cases, this symmetrization does not greatly alter the distribution, and, in such cases, the Preisach and FORC distributions are approximately equivalent. In most cases, however, this symmetrization alters the nature of the distribution. In these cases, the Preisach distribution is entirely distinct from a FORC distribution.

A Preisach distribution is a key component of the phenomenological model of interacting SD particles due to *Preisach* [1935] and *Néel* [1954]. In the Preisach model the interaction between particles is represented by a spatially fluctuating interaction field where it is assumed that this field is independent of the magnetization state of the sample. The physical basis of the Preisach model [*Néel*, 1954] is highly simplified compared with the physical reality of magnetization processes. Nevertheless, in some cases, this model is a reasonable approximation. The accuracy of the Preisach model can be tested by determining whether the Preisach distribution is magnetization-independent (or "statistically stable"). In fields not too near saturation, Preisach distributions seem to be approximately stable for some geological and synthetic samples [e.g., *Bate*, 1962; *Dunlop*, 1969; *Mullins and Tite*, 1973]. In cases where the Preisach distribution is apparently stable, the Preisach model can be used to predict magnetization and alternating field demagnetization curves of isothermal, anhysteretic and thermoremanent magnetizations [e.g., *Dunlop*, 1969; *Dunlop et al.*, 1990; *Hejda et al.*, 1994; *Dunlop and Özdemir*, 1997; *Fabian and von Dobeneck*, 1997]. However, because of the phenomenological nature of the Preisach model, the accuracy of the model will vary from one type of magnetic system to another and there are cases where the Preisach model is clearly inadequate [e.g., *Girke*, 1960]. The only case where the Preisach model can be considered truly precise is for a non-interacting, SD particle system at zero temperature (in this case, a Preisach distribution and a FORC distribution will be rigorously equivalent). Various improvements have been made to the Preisach model, notably the moving Preisach model [e.g., *Vajda and DellaTorre*, 1991]. Nevertheless, the moving Preisach model remains phenomenological and its accuracy will vary from one type of magnetic system to the next.

In contrast to Preisach distributions, FORC distributions do not involve any model-dependent assumptions or approximations. A FORC distribution is rigorously defined as a mathematical transformation of a suite of experimentally measured partial hysteresis curves. Our primary interest in acquiring FORC distributions is to characterize the magnetic particles within natural samples, rather than to force the distribution to fit a phenomenological model or to predict other types of magnetization curve. We therefore prefer to use the term "FORC distribution" to maintain and underscore these important distinctions between our approach and previous work with the Preisach model.

4. Interpretation of FORC Diagrams

In this paper, we focus on describing FORC diagrams for a wide range of well-characterized natural samples, along with a theoretical framework that helps to provide a basis for interpretation of features on FORC diagrams. This theoretical framework is described in more detail elsewhere [*Pike et al.*, 1999, 2000, also manuscript in preparation, 2000]. Our use of FORC diagrams in this paper is almost purely qualitative and descriptive rather than quantitative. To maximize the information that can be derived from FORC diagrams, it will be necessary to develop quantitative tools for analysis of FORC diagrams. This is beyond the scope of the present paper. Qualitative description of features on FORC diagrams, as demonstrated in this paper, indicates that the observed features are substantial, real and useful for obtaining a considerable amount of information that is unavailable from standard hysteresis measurements.

4.1 Noninteracting and Interacting SD Behavior

The behavior of noninteracting SD grains is well understood. A FORC distribution of noninteracting SD grains, at $T = 0$, with a log-normal distribution of volumes was calculated by *Pike et al.* [1999] (Figure 3a). The FORC distribution in Figure 3a is highly peaked on the $H_u = 0$ axis and the contours are elongated with negligible vertical spread. The small amount of observed vertical spread is due to the effects of numerical smoothing involved in calculating a FORC diagram. Modeling of SD particle systems with interactions is more difficult, but it is clear that interactions will produce FORC distributions with far greater vertical spread (Figures 3b and 3c). Figure 3b was produced by modeling the same assemblage of SD particles with a local interaction field that is assumed to be constant at a given particle site, but which varies randomly between particles [*Pike et al.*, 1999]. The large vertical spread in Figure 3b is due to this randomly varying local interaction field. The model was then modified [*Pike et al.*, 1999] to incorporate a stabilizing mean interaction field (where a stabilizing mean field acts parallel to the net magnetization of the sample). This mean field does not increase the vertical spread of the distribution (Figure 3c). Instead, it has moved the peak of the distribution below the $H_u = 0$ axis and has given the direction of contour elongation a positive slope (Figure 3c). It is therefore possible to distinguish between the effects of a mean interaction field and a randomly varying local interaction field.

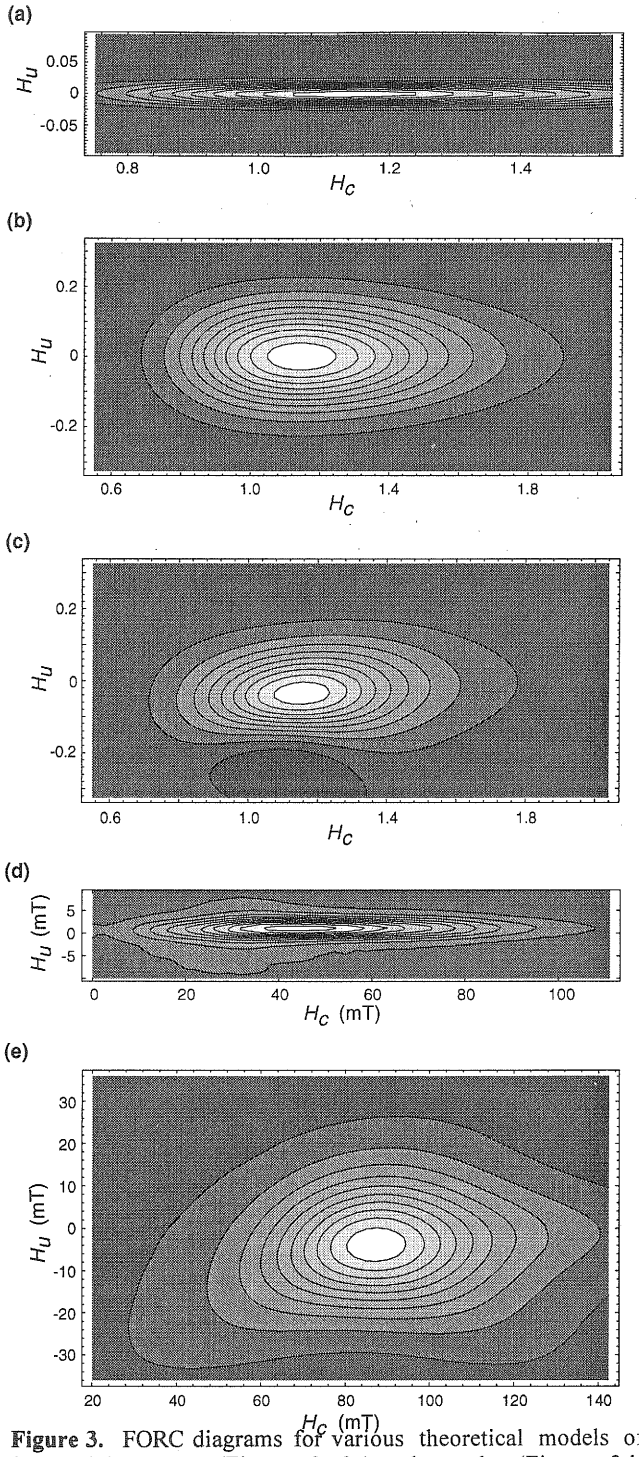

Figure 3. FORC diagrams for various theoretical models of SD particle systems (Figures 3a-3c) and samples (Figures 3d-3e). (a) FORC diagram for a theoretical model of noninteracting SD particles with log-normal grain size distribution. (b) FORC diagram for a system of SD particles with a local interaction field that is assumed to be constant at a given particle site but which varies randomly between particles. (c) FORC diagram for the same system of interacting SD particles after incorporation of a positive mean interaction field. Figures 3a-3c are after *Pike et al.* [1999]. (d) FORC diagram for sample CS911 from the Yucca Mountain ash flow tuff from southern Nevada (see text). (e) FORC diagram for a floppy disk sample, of which the data in Figure 1b are a subset. The FORC diagrams are shown to scale (i.e., the vertical and horizontal scales are identical).

The theoretical models illustrated in Figures 3a-3c provide a basis for interpretation of empirical data. Based on these results, we can infer that a sample from the titanomagnetite-bearing Yucca Mountain ash flow tuff (CS911) from southern Nevada [*Eick and Schlinger*, 1990; *Worm*, 1999] (Figure 3d; M_r/M_s = 0.51, H_{cr}/H_c = 1.23) contains noninteracting SD particles. The contours on the FORC diagram (Figure 3d) have negligible vertical spread and are similar to those for a model of noninteracting SD particles (Figure 3a). The lack of magnetic interactions in this sample is attributed to growth of titanomagnetite by nucleation within volcanic glass at elevated temperatures, subsequent to emplacement of the Yucca Mountain ash flow tuff [*Schlinger et al.*, 1988].

Based on a comparison with Figure 3c, we can also infer that a typical magnetic floppy disk (Figure 3e) has a substantial random local interaction field (indicated by vertical spread of the contours) and a stabilizing mean interaction field (indicated by displacement of the distribution peak below the H_u = 0 axis and a positive slope of the line of contour elongation). In addition, the peak of the distribution indicates a mean coercivity of 88 mT for the SD particles in the floppy disk. As expected for high-fidelity iron oxide floppy disks, this coercivity is much higher than those encountered in (titano-)magnetite-bearing geological samples (compare with Figure 3d).

FORC diagrams for geological samples with interacting SD particles are shown in Figure 4. The samples include a (titano-) magnetite-bearing sample (CRB-15) from the Columbia River Basalt [*Smith and Verosub*, 1994] (Figure 4a; M_r/M_s = 0.68, H_{cr}/H_c = 1.04); an early Miocene glaciomarine sediment from Antarctica (CRP-1-145.46) with unknown mineralogy but relatively high coercivity [*Roberts et al.*, 1998] (Figure 4b; M_r/M_s = 0.56, H_{cr}/H_c = 1.36); and a greigite-bearing late Pliocene lake sediment (BV1438) from Butte Valley, northern California [*Roberts et al.*, 1996] (Figure 4c; M_r/M_s = 0.51, H_{cr}/H_c = 1.38).

FORC diagrams for natural SD samples (Figure 4) can also be interpreted with the help of the theoretical results of *Pike et al.* [1999]. The vertical spread in these FORC distributions is a manifestation of magnetostatic interactions, while the H_c coordinate at the peak of each distribution is a measure of the mean switching field of the SD particle assemblages. It is clear that sample CRB-15 (Figure 4a) is dominated by a different mineral than sample BV1438 (Figure 4c). The value of H_c at the peak of the distribution is ~20 mT and 64 mT for CRB-15 and BV1438, respectively. These values are typical of the mean coercivity of SD magnetite [*Dunlop and Özdemir*, 1997] and SD greigite [*Roberts*, 1995], respectively.

We are accustomed to thinking of floppy disks as containing strongly interacting SD particles. However, by comparing the FORC diagram contours for the floppy disk (Figure 3e) with those of Figure 4, it is clear that interactions in these natural samples are about half as strong as in the floppy disk. Such strong interactions will have a significant effect on the hysteresis ratios [e.g., *Sprowl*, 1990]. Magnetic interactions seem to be the most likely explanation for lowering the M_r/M_s ratios for each of these samples below the values expected for materials with magnetocrystalline anisotropy [e.g., *Chikazumi*, 1964; *Dunlop and Özdemir*, 1997]. In addition to the randomly varying local interaction field, the fact that the peak of the distributions for these samples lies below the H_u = 0 axis (Figure 4) indicates that the

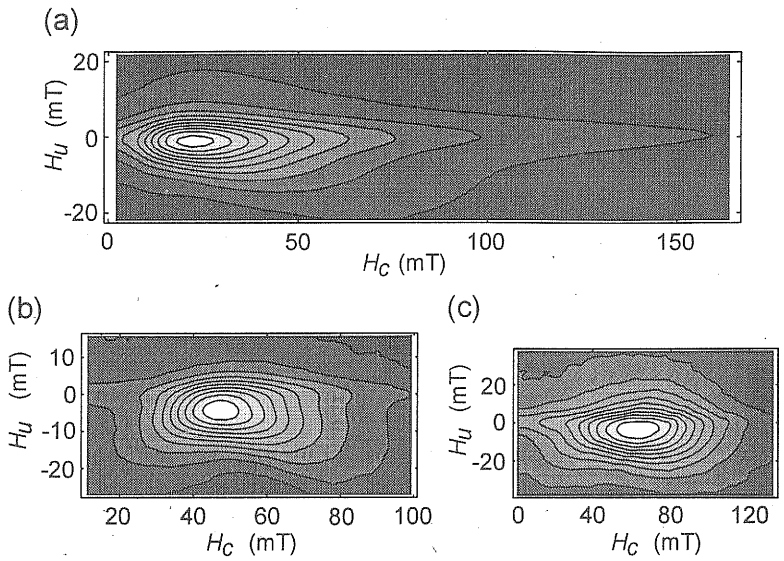

Figure 4. FORC diagrams for geological samples containing interacting SD particles. (a) FORC diagram for sample CRB-15 from the Columbia River Basalt (see text). (b) FORC diagram for sample CRP-1-145.46 from Miocene glaciomarine sediments, Antarctica (see text). (c) FORC diagram for sample BV1348 from Pleistocene lake sediments, northern California (see text).

particles are also affected by a stabilizing mean interaction field. These results for noninteracting and interacting SD particle systems indicate that qualitative interpretation of FORC diagrams provides considerable assistance with understanding the magnetic properties of natural samples.

4.2 Superparamagnetic Behavior

The theoretical models of SD behavior described above (Figure 3a-c) were all calculated for $T = 0$. In an assemblage of SD particles at $T > 0$, thermal relaxation effects can give rise to superparamagnetism. The magnetization of SP particles is entirely reversible and reduces to zero when the derivative is taken with respect to H_a in equation (1). Thus, SP particles would not be expected to produce any manifestation on a FORC diagram. However, particles at or just below the SP threshold volume at room temperature will behave in a quasi-reversible manner. That is, when the applied field switches direction there will be a small but detectable relaxation time as these particles overcome their energy barriers and switch direction. Consider two FORCs: an upper FORC with H_a just greater than zero, and a lower FORC with H_a just less than zero. At the reversal point of the lower FORC ($H_a < 0$), some of these quasi-SP particles will have reversed (where these particles are not reversed on the upper curve). As the applied field is increased from H_a, the magnetization on the lower FORC will briefly lag behind the upper FORC due to the relaxation effect described above. The small difference between these two FORCs will create a non-zero result when calculating the derivative with respect to H_a in equation (1). The result is a contribution to a FORC distribution that is located at H_a, $H_b = 0$ (i.e., about the origin of a FORC diagram at H_u, $H_c = 0$).

As illustrated by the following results from geological samples, secondary peaks are often observed about the origin of FORC diagrams. FORC diagrams for a carbonate-rich marine sediment (sample ODP 747A-7X-3-37) from the Kerguelen Plateau, which contains disseminated volcanic ash particles from the Kerguelen igneous province, including SD magnetite ($M_r/M_s = 0.42$; $H_{cr}/H_c = 2.64$) [*Heider et al.*, 1993], are shown in Figures 5a and 5b. FORC diagrams from magnetite-bearing early Pleistocene lake sediments (sample BV1126) from Butte Valley, northern California [*Roberts et al.*, 1996], are shown in Figures 5c and 5d. Sample BV1126 displays wasp-waisted hysteresis behavior, which, in this case, was identified as being due to a mixture of SD and SP magnetite [*Roberts et al.*, 1995b].

For sample ODP 747A-7X-3-37, the contours on the conventional FORC diagram (Figure 5a) appear to indicate a peak of the FORC distribution near the origin of the plot. To resolve the features of the FORC distribution in this area, a more detailed diagram (Figure 5b) was obtained by using a finer field spacing between successive FORCs (0.7 mT instead of 3 mT for Figures 5b and 5a, respectively). High-resolution FORC diagrams are useful for focusing on different areas of interest in a FORC distribution. Figure 5b has a peak centered on the $H_u = 0$ axis at 23 mT which is not clearly evident in Figure 5a. This value of $H_c = 23$ mT is consistent with a dominance of magnetite. The narrow, elongated contours in Figure 5b, by analogy with the model in Figure 3a and the empirical results in Figure 3d, indicate the presence of noninteracting SD particles. If interactions were present, these contours would have greater vertical spread and the contours would not be centered on the $H_u = 0$ axis. The small ">"-shaped contours located immediately about the origin of the FORC diagram (Figure 5b) indicate that the distribution has been shifted to lower coercivities by thermal relaxation effects. The secondary peak at the origin of the FORC diagram therefore appears to be a hallmark of particles that have lost their coercivity (i.e., SP particles).

The ability to identify the presence of interactions and SP material using FORC diagrams enables us to resolve ambiguities in interpretation of hysteresis parameters. For example, the M_r/M_s ratio for sample ODP 747A-7X-3-37 (0.42) is lower than expected for an assemblage of noninteracting SD particles. Interactions in this sample are

negligible (Figure 5b), and the presence of SP particles is the most likely explanation for the observed reduction in the M_r/M_s ratio. FORC diagrams also help to resolve ambiguities for sample BV1126. In the normal-resolution FORC diagram for sample BV1126, SD and SP contour peaks are both evident (Figure 5c). The details of these features are more clearly resolved in the high-resolution FORC diagram (Figure 5d). This FORC diagram is similar to that for sample ODP 747A-7X-3-37 (Figure 5b) except that the peak of the distribution is displaced to lower coercivities (the peak is at H_c = ~17 mT).

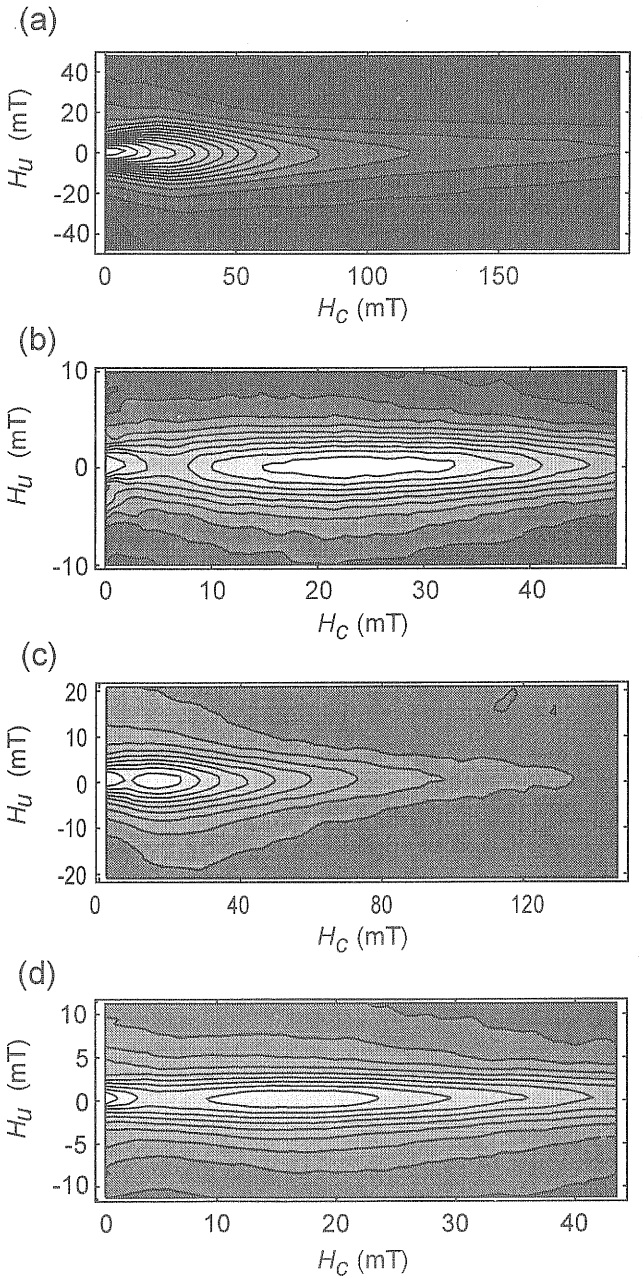

Figure 5. FORC diagrams for natural samples that contain SP and non-interacting SD grains. (a) Normal-resolution FORC diagram for sample ODP 747A-7X-3-37 from the Kerguelen Plateau (see text). (b) High-resolution FORC diagram for sample ODP 747A-7X-3-37. (c) Normal-resolution FORC diagram for sample BV1126 from early Pleistocene lake sediments, northern California (see text). (d) High-resolution FORC diagram for sample BV1126.

This indicates that thermal relaxation effects are more significant for sample BV1126. It is therefore likely, as suggested by *Roberts et al.* [1995b], that the wasp-waisted behavior exhibited by sample BV1126 is due to significant contributions from both SP and noninteracting SD particles.

In order to test whether the secondary peaks near the origin of the FORC diagrams in Figures 5b and 5d are due to the presence of SP particles, we analyzed a sample for which the magnetic fraction is known to be dominated by SP particles [*Worm*, 1998, 1999; *Worm and Jackson*, 1999]. The sample (CS914) is from the same Yucca Mountain ash flow tuff sequence as sample CS911, as described above [*Schlinger et al.*, 1988; *Eick and Schlinger*, 1990]. It is difficult to provide estimates of H_c, H_{cr}, and M_r/M_s for this sample because these parameters depend sensitively on measurement timescales due to the large SP content. However, the frequency dependence of magnetic susceptibility is exceptionally high (30%) [*Worm*, 1998, 1999] and clearly indicates the presence of a large fraction of SP particles. The FORC distribution for sample CS914 (Figure 6a) contains no separate peak due to SD particles. Instead, the distribution has a large peak centered about the origin of the FORC diagram. This FORC distribution (Figure 6a) provides evidence that the peak at the origin of a FORC diagram is a real effect in samples containing SP particles, and is not an artifact of our measurement procedure.

An Aptian red bed sample from the south of France (90-VAU-42) also contains a significant SP content in addition to SD magnetite and SD hematite. The FORC distribution for this sample (Figure 6b) contains a secondary peak near the origin of the plot, as well as vertical contours immediately adjacent to the H_u axis in the lower half plane. *Pike et al.* [2000] calculated FORC distributions from numerical models of noninteracting, uniaxially anisotropic SD particles, including thermal relaxation effects. The results of these theoretical models reproduce the features observed in both of the FORC distributions shown in Figure 6. In these calculations, increasing temperature produces thermal relaxation and shifts the distribution peak toward lower coercivities. At sufficiently high temperatures, the SD peak of the FORC distribution disappears, as observed for natural samples that contain a large proportion of SP material (e.g., Figure 6a). Vertical contours in the lower left-hand portion of the FORC diagram that lie nearly parallel to the H_u axis (Figure 6b) are also produced as a result of thermal relaxation in these calculations. The vertical contours result from a slight relaxation of the magnetization on FORCs just after the applied field has begun increasing from the reversal field [*Pike et al.*, 2000]. These results help to provide a solid theoretical basis for interpretation of SP effects on FORC diagrams from natural samples.

4.3 MD and PSD Behavior

In contrast to systems of SD particles, it is more difficult to develop a theoretical framework for understanding the manifestations of MD and PSD particles on FORC diagrams. The main problem is that the physical mechanisms that generate hysteresis in MD and PSD particles are not well understood [*Dunlop and Özdemir*, 1997]. In the following discussion, we emphasize our empirical results before trying to explain the manifestations of MD particles on FORC diagrams.

Samples that are dominated by MD particles produce characteristic contours that diverge away from the origin of a FORC diagram (Figure 7). Similar diverging contour patterns have

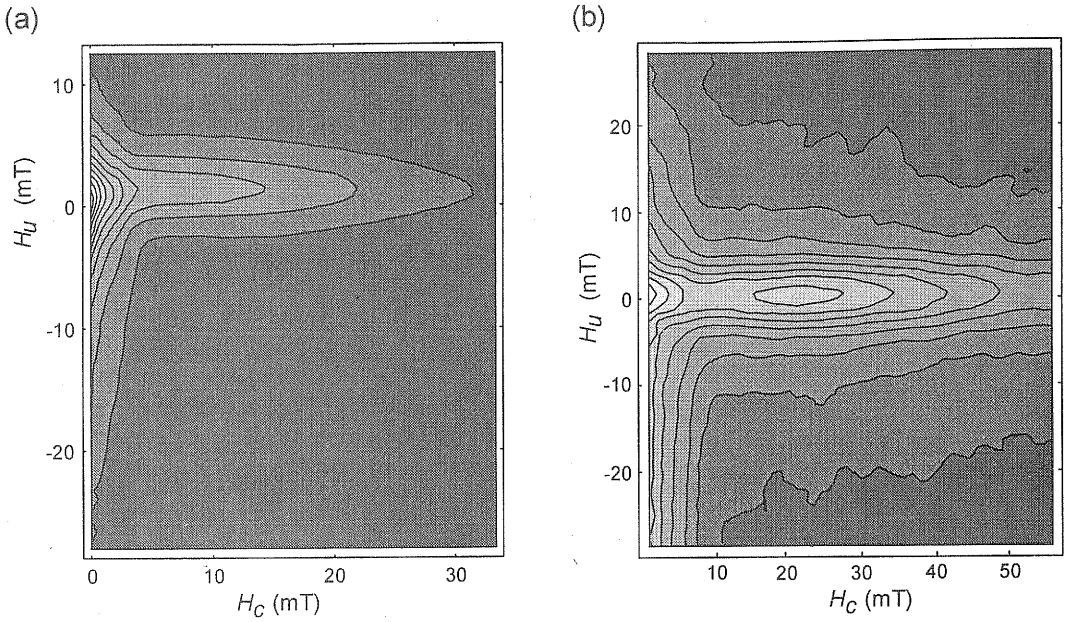

Figure 6. FORC diagrams for natural samples that contain substantial SP components. (a) FORC diagram for sample CS914 from the Yucca Mountain ash flow tuff in southern Nevada (see text). (b) FORC diagram for sample 90-VAU-42 from Cretaceous red sediments in France (see text).

also been observed in Preisach diagrams for natural samples [e.g., *Mullins and Tite*, 1973; *Ivanov et al.*, 1981; *Ivanov and Sholpo*, 1982; *Zelinka et al.*, 1987; *Hejda and Zelinka*, 1990; *Dunlop et al.*, 1990; *Fabian and von Dobeneck*, 1997]. Despite the fact that these contours have considerable vertical spread, the contour patterns are completely different to those of interacting SD particle systems (Figures 3b and 3c). Interacting SD systems have contours that close about a central peak, whereas the MD FORC distributions (Figure 7) have no such peak and the contours diverge from the $H_u = 0$ axis and intersect the $H_c = 0$ axis. It is difficult to see how interactions produce this divergence, especially when the contours are centered close to the $H_u = 0$ axis (which indicates that interactions are negligible).

It is noteworthy that the peaks of the FORC distribution in Figures 7-9 are displaced slightly above the $H_u = 0$ axis. This slight offset occurs because, during a FORC measurement, the applied field cannot be changed instantaneously and more time is spent at the reversal point (H_a in Figure 1a) than at any subsequent point on a FORC. Due to magnetic viscosity effects, the pause at H_a will provide an effective downward shift of the reversal field which will cause an upward shift of the FORC distribution, as evident in Figures 7-9. *Pike et al.* [1999, 2000] demonstrated this effect by adding a longer pause at the reversal field which produced a greater upward shift of the FORC distribution. This upward offset is only obvious in the absence of magnetic interactions. When interactions are present, this effect is overwhelmed and the FORC distribution is offset below the $H_u = 0$ axis (e.g., Figures 3e and 4).

Upon first inspection, it might be thought that there is a similarity between the sets of divergent FORC distribution contours from samples dominated by SP and MD particles. However, comparison of Figures 6 and 7 indicates that the two types of samples have distinctly different behavior. The diverging contours due to SP particles lie close to the origin, at H_c values that are always much <10 mT, whereas the FORC distributions for MD particles have diverging contours that usually extend beyond 30 mT. Furthermore, the contours for SP particles are usually much steeper than those for natural MD particles and are much more pronounced in the lower left-hand portion of the FORC diagram. By contrast, FORC distributions for natural MD samples are nearly symmetrical (Figure 7). Thus, despite the fact that MD and SP particles both produce contours that diverge away from the origin of a FORC diagram, the nature of the contours is distinctly different and they can be readily distinguished from each other.

The natural samples shown in Figure 7 include: a detrital carbonate layer (sample DC4) that corresponds to Heinrich layer 4 from a piston core from the Labrador Sea [*Stoner et al.*, 1996] (Figure 7a; $M_r/M_s = 0.07$, $H_{cr}/H_c = 6.72$); a clay-rich late Pleistocene sediment with abundant ice-rafted detritus (sample ODP 887B-2H-6-70) from the North Pacific Ocean [*Roberts et al.*, 1995a] (Figures 7b and 7c; $M_r/M_s = 0.09$, $H_{cr}/H_c = 4.89$); and a sample of the Azuki volcanic ash (KSAZD2) which is intercalated with the Kobiwako Group at a locality on the Kisen River on the western shore of Lake Biwa, Japan [*Hayashida et al.*, 1996] (Figure 7d; $M_r/M_s = 0.16$, $H_{cr}/H_c = 3.46$).

The natural MD samples display similar behavior, as would be expected because each sample is dominated by (titano-) magnetite [cf. *Roberts et al.*, 1995a; *Hayashida et al.*, 1996; *Stoner et al.*, 1996]. A high-resolution FORC diagram for sample ODP 887B-2H-6-70 (Figure 7c) indicates that there is no SD peak and that all but the inner two contours display the divergent pattern that is characteristic of MD grains. Sample KSAZD2 displays somewhat different behavior to the MD samples (Figure 7d). While the outer contours display the characteristic divergent pattern, the inner contours are somewhat less divergent, and the FORC diagram is less symmetrical than those for MD samples. The FORC diagram shown in Figure 7d seems to be characteristic of PSD behavior (see below).

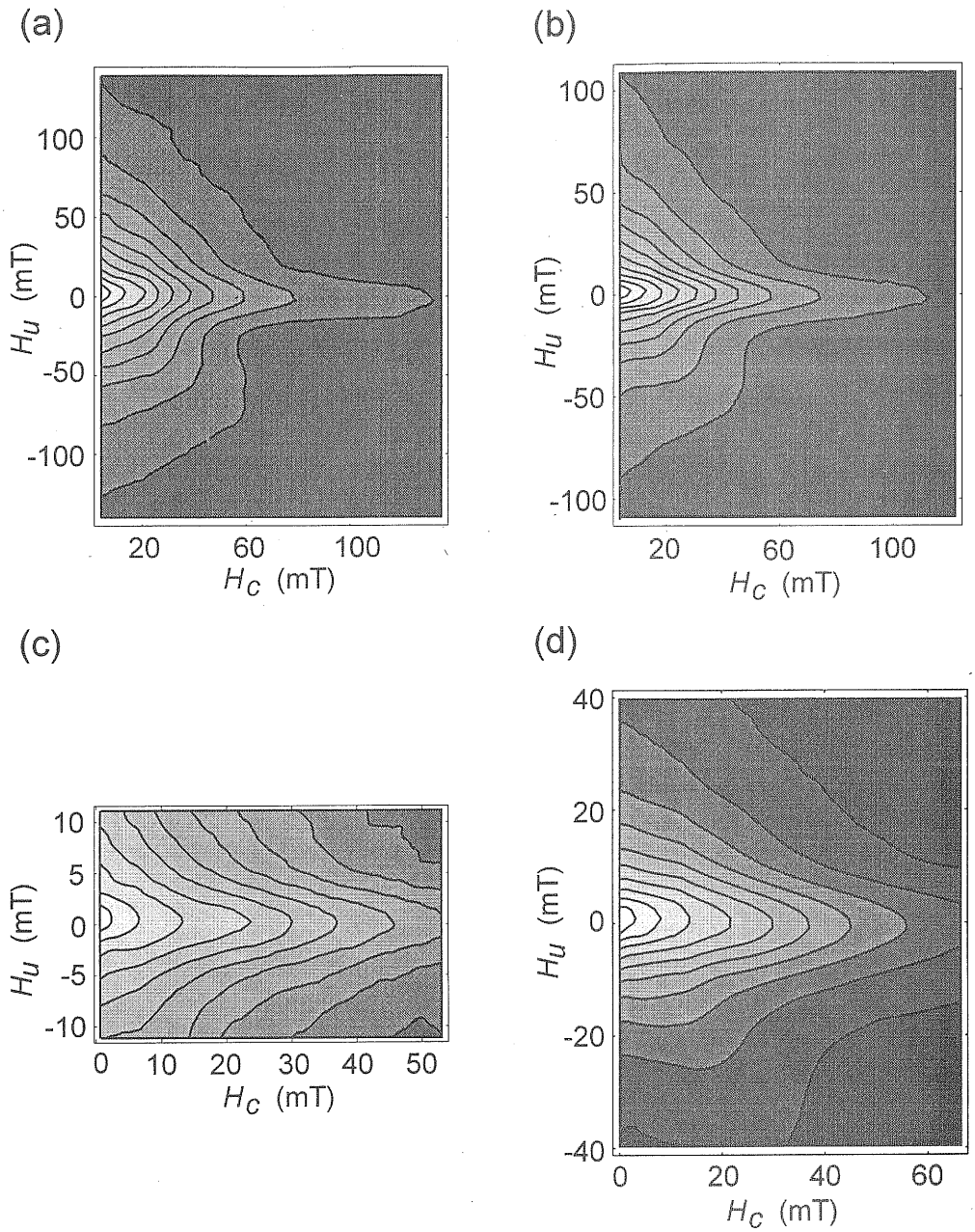

Figure 7. FORC diagrams for natural samples that contain MD (Figures 7a-7c) and PSD (Figure 7d) grains. (a) FORC diagram for sample DC4 from the Labrador Sea (see text). (b) Normal-resolution FORC diagram for sample ODP 887B-2H-6-70 from the North Pacific Ocean (see text). (c) High-resolution FORC diagram for sample ODP 887B-2H-6-70. (d) FORC diagram for sample KSAZD2 from near the western shore of Lake Biwa, Japan (see text).

The physical mechanisms that give rise to the diverging MD contour patterns are presently unknown. The two mechanisms that are most frequently invoked in discussions of MD hysteresis are domain wall (DW) pinning and DW nucleation and annihilation. With both of these mechanisms, increased grain size would lead to increased vertical spread on a FORC diagram, which is consistent with our data. However, it is not clear how either of these mechanisms could give rise to the diverging contour patterns observed for natural MD assemblages. The classical DW pinning model of *Néel* [1955] predicts perfectly vertical contours on a FORC diagram, and a FORC distribution that is a decreasing function of H_c [*Bertotti et al.*, 1999]. We have shown that the predictions of the classical DW pinning model are consistent with experimental FORC diagrams for a bulk sample of transformer steel and for large (2 mm) individual magnetite grains (*C. R. Pike et al.*, manuscript in preparation, 2000). However, this model does not help to explain the diverging contours observed for smaller natural MD particle assemblages. It is not known what physical mechanism is responsible for the breakdown of the classical DW pinning model in smaller grains. If, in the future, the classical DW pinning model is modified to account for DW interactions and DW curvature, it might be possible to explain the diverging contour patterns. Alternatively, it might be

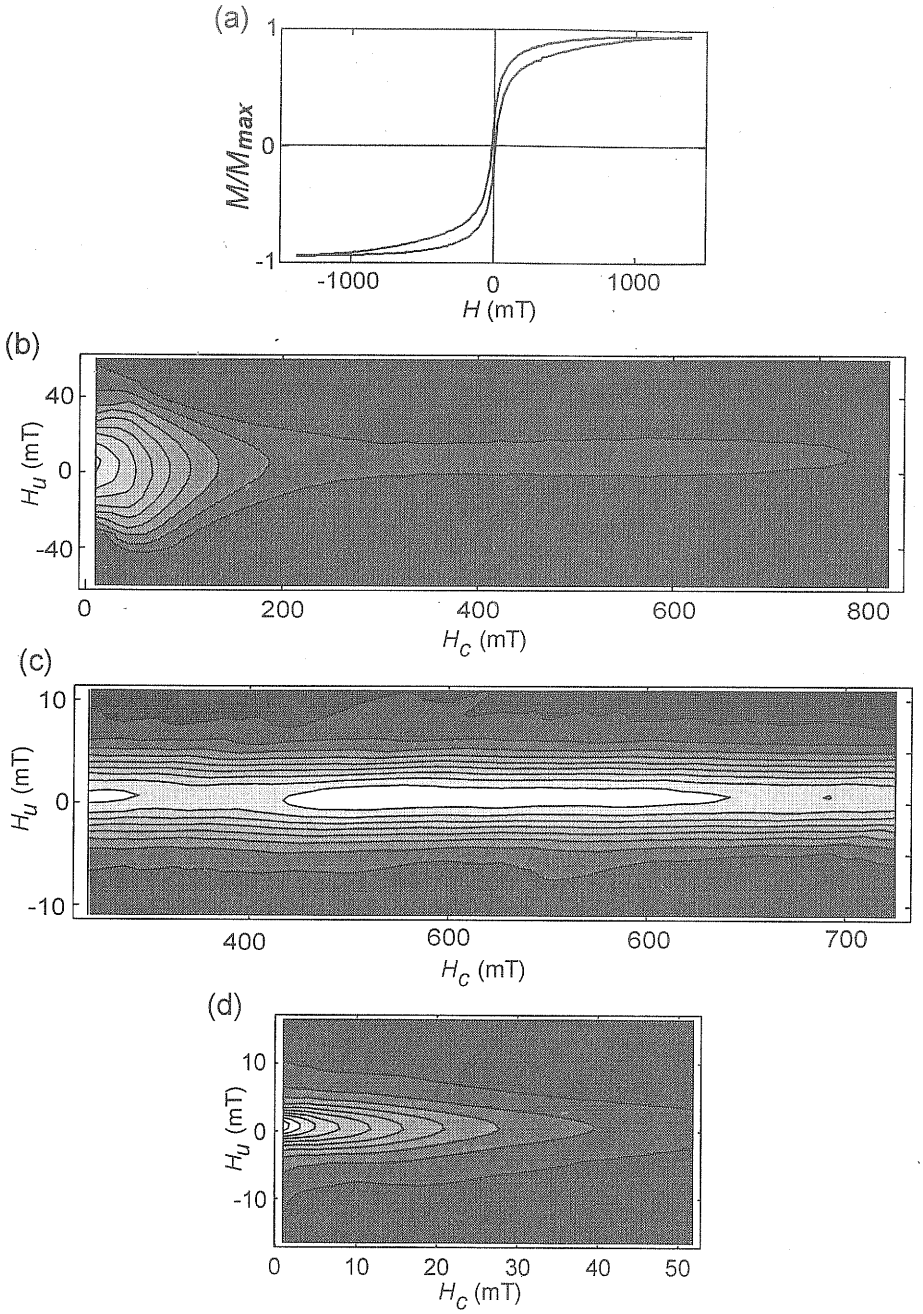

Figure 8. Example of the use of FORC diagrams to elucidate mixed magnetic assemblages. The sample is from a brick from a medieval Bulgarian church. (a) Wasp-waisted hysteresis loop from sample BULG1371. (b) Normal-resolution FORC diagram which shows the range of coercivities of particles in sample BULG1371. (c) High-resolution FORC diagram for the high-coercivity component of sample BULG1371 (note that the vertical scale is distorted for the sake of illustration). (d) High-resolution FORC diagram for the low-coercivity component of sample BULG1371 (see text for discussion).

necessary to introduce a new type of model for MD hysteresis based on DW nucleation and annihilation. Further work is required to resolve these uncertainties.

5. Applications of FORC Diagrams

Through the above examples, and by comparison with the interpretive framework provided by our theoretical models, it is evident that FORC diagrams can be used to obtain a more detailed interpretation of magnetic assemblages than is possible with standard hysteresis parameters. The effects of thermal relaxation (i.e., superparamagnetism), variations in domain state and magnetic interactions all produce characteristic and distinct manifestations on a FORC diagram. In the remainder of this paper, we illustrate three applications of FORC diagrams in discriminating magnetic components from natural samples.

5.1 Using FORC Diagrams to Elucidate Mixed Magnetic Assemblages

Wasp-waisted hysteresis loops often occur as a result of the presence of two or more coexisting magnetic components with strongly contrasting coercivities [e.g., *Wasilewski*,

1973; *Jackson*, 1990; *Channell and McCabe*, 1994; *Roberts et al.*, 1995b, *Tauxe et al.*, 1996]. We have tested the usefulness of FORC diagrams by analyzing samples with wasp-waisted hysteresis behavior. Sample BULG1371 [*Kovacheva*, 1997] is from a brick from a medieval (14th century) Bulgarian church. The wasp-waisted hysteresis loop (Figure 8a) has a significant high-coercivity component and the loop does not fully saturate at applied fields of 1.4 T. The peak of the FORC distribution for this sample is centered near the origin of the FORC diagram, but there is also a contour that extends toward very high coercivities to the right of the diagram (Figure 8b). High-resolution FORC diagrams were obtained for both the high- and low-coercivity components. The high-coercivity component (Figure 8c) has a peak at ~530 mT: the contours that define this peak have little vertical spread and are centered on the $H_u = 0$ axis, which indicates that magnetic interactions are negligible. Based on high-temperature data, *Roberts et al.* [1995b] concluded that this high-coercivity component is due to the presence of goethite. The mean coercivity of ~530 mT is consistent with published coercivities for goethite [*Dekkers*, 1989]. The low-coercivity contours (Figure 8d) intersect the $H_c = 0$ axis but do not diverge away from the $H_u = 0$ axis. As was observed for sample KSAZD2 (Figure 7d), we interpret this type of contour pattern to indicate the presence of PSD grains.

As concluded by *Roberts et al.* [1995b], the wasp-waisted hysteresis behavior of this sample results from the contrast in coercivities between goethite and magnetite. However, the FORC diagrams provide much more specific information because they confirm that the goethite occurs as non-interacting SD grains and that the magnetite occurs as PSD grains. This example, in addition to results from sample BV1126, as discussed above (Figures 5c and 5d), indicates that FORC diagrams provide a powerful means of discriminating between different components in mixed magnetic assemblages.

5.2 Using FORC Diagrams to Elucidate the Results of Sequential Leaching Techniques

Sequential leaching techniques, such as citrate-bicarbonate-dithionate (CBD) treatments [*Mehra and Jackson*, 1960], are commonly used by soil chemists to remove iron oxides from

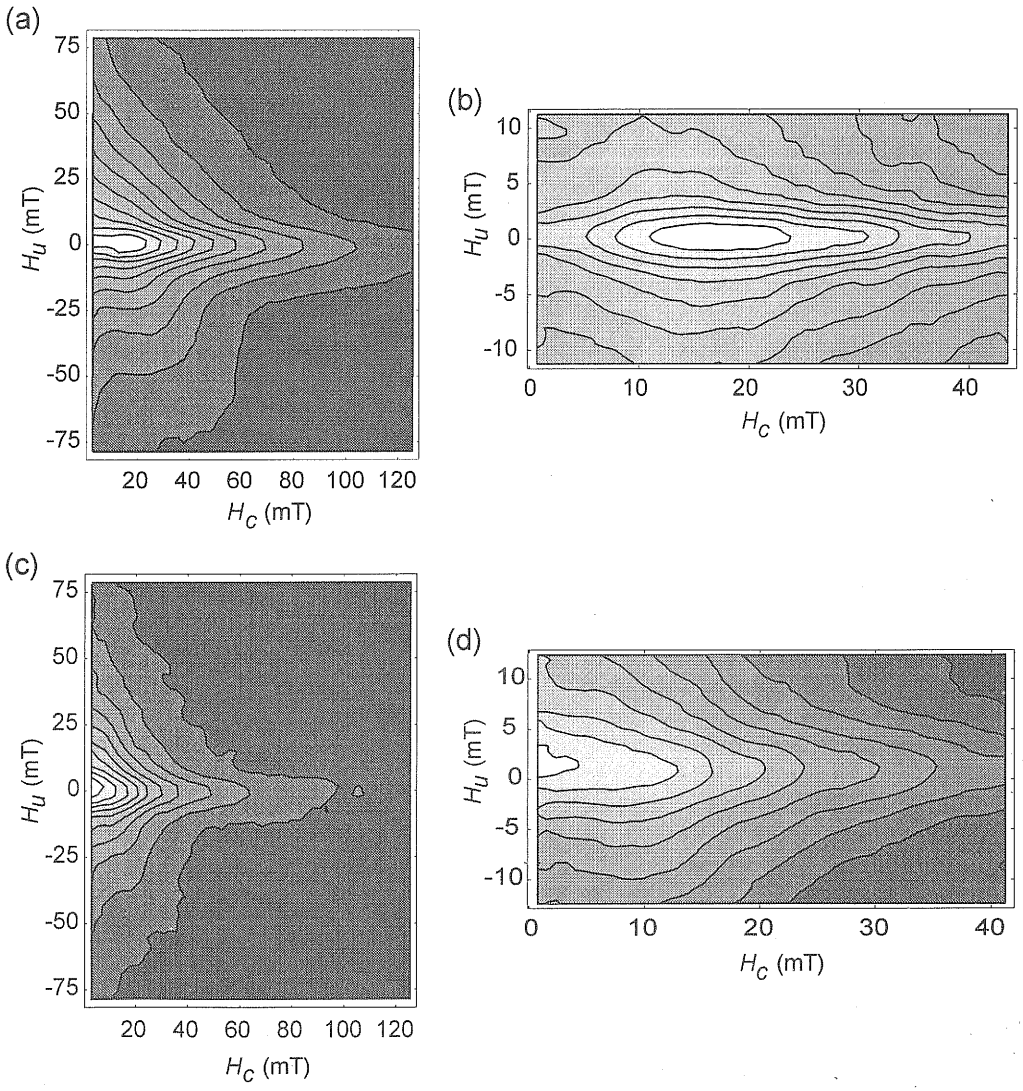

Figure 9. Example of the use of FORC diagrams to elucidate the results of sequential leaching techniques. The sample is from Gucheng Lake, China. (a) Normal-resolution FORC diagram for sample G71 before CBD treatment. (b) High-resolution FORC diagram for sample G71 before CBD treatment. (c) Normal-resolution FORC diagram for sample G71 after CBD treatment. (d) High-resolution FORC diagram for sample G71 after CBD treatment (see text for discussion).

samples to facilitate clay mineral analysis. More recently, the CBD method has been used to study the contribution of fine-grained pedogenic magnetite to the magnetization of Chinese loess/paleosol sequences [e.g., *Verosub et al.*, 1993]. We applied the CBD technique to sediments from Gucheng Lake, China (sample G71) [*Wang et al.*, 1999], and obtained FORC diagrams for the sample before and after CBD treatment. Prior to CBD treatment, sample G71 clearly has a MD component (Figure 9a), as indicated by the diverging contours on the FORC diagram (compare with Figure 7). A high-resolution FORC diagram also indicates a peak that represents noninteracting SD grains (Figure 9b). The coercivity of the SD component is consistent with that of magnetite. The hysteresis loop is not visually distorted, despite the presence of these two components (M_r/M_s = 0.14, H_{cr}/H_c = 3.36). CBD treatment is expected to dissolve the finest-grained iron oxide component within the sample. This is exactly what is seen in the FORC diagram for sample G71 after CBD treatment. The magnetization is reduced and the signal/noise ratio is decreased. Thus, using the same *SF* value as for the original sample, the resulting FORC diagram is more noisy (Figure 9c). Nevertheless, it is clear that all of the contours diverge away from the H_u = 0 axis and intersect the H_c = 0 axis. The high-resolution FORC diagram confirms that only MD grains remain after CBD treatment (Figure 9d), which is consistent with the standard hysteresis parameters (M_r/M_s = 0.09, H_{cr}/H_c = 3.88). Removal of the SD component during CBD treatment has clearly shifted all of the contours to lower coercivities (compare Figures 9a and 9c).

These results provide a useful demonstration of the interpretive value of FORC diagrams. Before CBD treatment, it was unclear whether the PSD-like hysteresis values (M_r/M_s = 0.14, H_{cr}/H_c = 3.36) resulted from PSD behavior or from a mixture of grain sizes. After examination of the FORC diagrams (Figures 9a and 9b), it appears that two grain size fractions were present in the lake sediment: a dominant MD component as well as a SD component.

5.3 Using FORC Diagrams to Check the Reliability of "Day" Diagrams

If standard hysteresis values were used to represent the domain state of the above-described Chinese lake sediments [cf. *Day et al.*, 1977], the results would be misleading because these samples contain a mixture of grain sizes. The possibility of using FORC diagrams to discriminate between different grain size components could be valuable for testing, on a case-by-case basis, whether it is appropriate to present hysteresis data in a "Day" diagram.

In Figure 10, we show a Day diagram for regularly-spaced samples from a Pleistocene sedimentary sequence from the Gulf of Alaska (ODP Hole 887B) that is dominated by clay; ice-rafted detritus and diatoms [*Roberts et al.*, 1995a]. The hysteresis data have considerable spread between the fine end of the PSD range and coarse MD values [cf. *Day et al.*, 1977]. FORC diagrams have been obtained for selected samples along the trend from "PSD" to "MD" values, as indicated by the open symbols on the Day diagram (Figure 10). There are clear differences between the FORC diagrams for samples along the "grain size" spectrum from ODP Hole 887B. MD behavior is clearly evident toward the coarse end of the observed spectrum (Figure 10d; compare with Figure 7). At the fine end of the spectrum, the FORC distributions appear to have a mixed set of contours. For Figure 10a, only the outer contours of the FORC distribution have a divergent pattern that would be expected for MD particles; the inner contours close about a central peak, as would be expected for noninteracting SD particles (this is particularly evident in the high-resolution FORC diagram). In addition, the high-resolution FORC diagram contains a secondary peak near the origin of the FORC diagram (Figure 10a) which indicates the presence of SP particles. The sample shown in Figure 10a therefore contains a mixed grain size assemblage and may not be suitable for presentation on a "Day" plot. The samples shown in Figures 10b and 10c contain greater evidence of MD particles (i.e., they have divergent contours), but the high-resolution FORC diagrams also contain SD peaks. There is a marked progression toward lower coercivities of the SD peaks for the samples shown in Figures 10a, 10b, and 10c (17, 13, and 9 mT, respectively). For the MD sample shown in Figure 10d, the SD peak has completely disappeared. Using Preisach diagrams, *Dunlop et al.* [1990] reported a similar progression of decreased coercivities of a SD peak through a range of PSD grain sizes. As argued by *Dunlop et al.* [1990], the closed and divergent contours probably represent the presence of both SD-like and MD-like magnetizations, respectively, within PSD grains. The mechanism of PSD behavior is still far from certain and the existence of SD-like components in the magnetization of small MD grains, in addition to ideal MD remanence, is widely accepted [e.g., *Xu and Dunlop*, 1994; *Dunlop and Özdemir*, 1997]. It is therefore likely that ambiguity will continue to exist when attempting to discriminate PSD behavior from that due to mixtures of SD and MD particles. However, the clear progression of decreased coercivitites of the SD-like component with increasing apparent grain size in the FORC diagrams in Figure 10 might be a hallmark of PSD behavior. This possibility should be considered in further attempts to test the usefulness of FORC diagrams for characterizing PSD behavior.

The use of sequential leaching techniques could also prove to be useful in resolving the ambiguity described above concerning PSD behavior. CBD treatment would be expected to dissolve SD particles in a sample containing mixtures of SD and larger grains (e.g., Figure 9). If the SD peak is still present after CBD treatment, it might indicate that the peak is due to SD-like behavior within larger PSD/MD particles. These speculations remain to be tested, and it is clearly necessary to develop an improved understanding of both PSD behavior and the manifestations of PSD particles on FORC diagrams.

6. Conclusions

A detailed understanding of the grain size distribution of a magnetic assemblage is often critically important in paleomagnetic and environmental magnetic studies. Techniques that enable measurement of bulk geological samples are preferable to those that require extraction of magnetic particles because the magnetic extract may not be representative of the full range of particles that contribute to the magnetization of the sample. In addition, magnetostatic interactions will be higher in magnetic extracts, and this could contribute to results that differ from those obtained from bulk samples. FORC diagrams appear to be a promising tool for developing an understanding of the magnetic grain size distribution of bulk natural samples. Through use of FORC diagrams, it is possible to discrim-

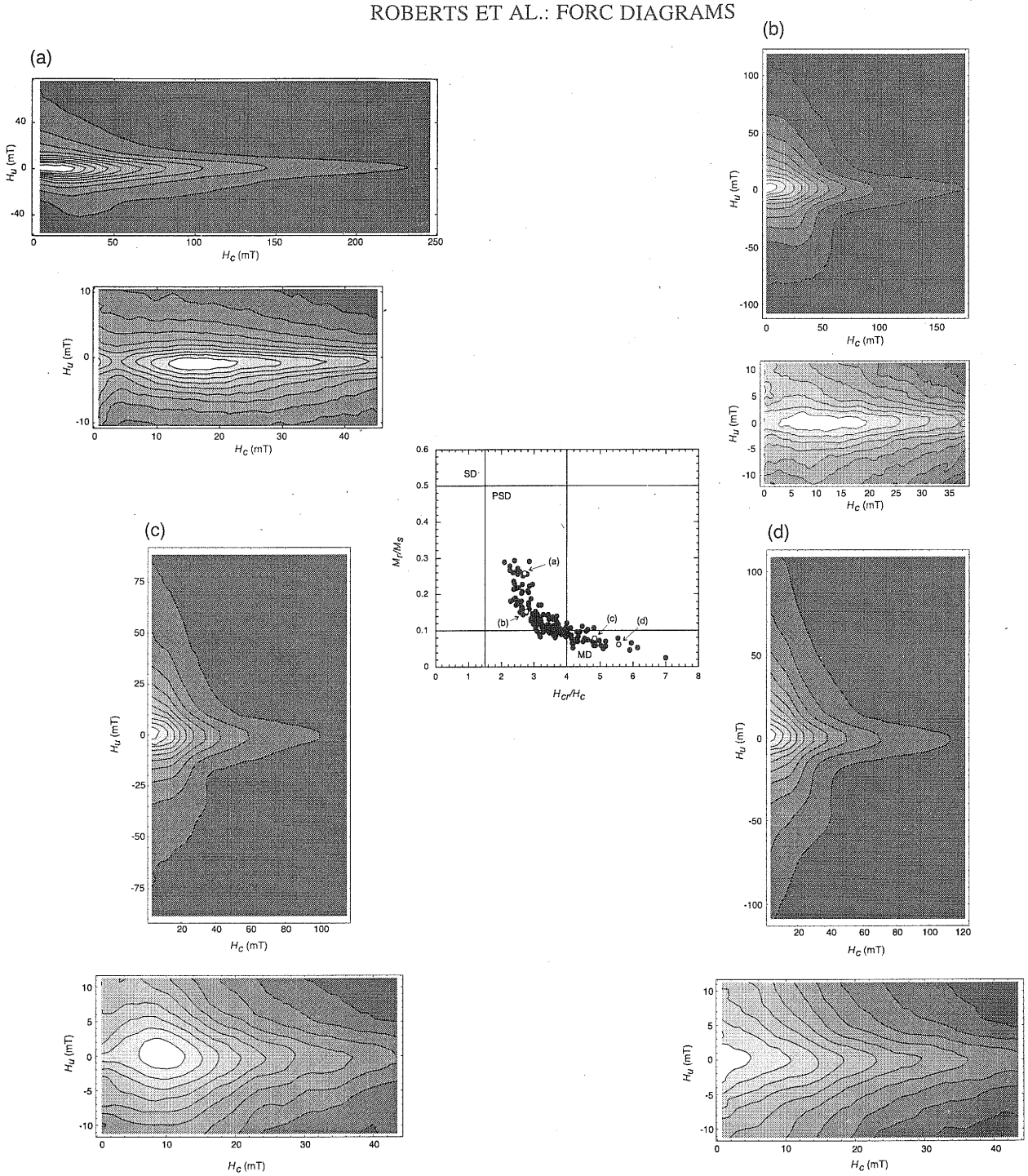

Figure 10. Example of the use of FORC diagrams to test the reliability of "Day" diagrams. Day plot of M_r/M_s versus H_{cr}/H_c (middle) for a suite of Pleistocene sediments from the northeast Pacific Ocean (ODP Hole 887B). FORC diagrams have been obtained for selected samples along the trend from "PSD" to "MD" values, as indicated by open symbols on the Day plot. (a) Sample ODP-887B-3H-2-30; (b) sample ODP-887B-2H-2-130; (c) sample ODP-887B-2H-2-90; and (d) sample ODP-887B-2H-6-20. For each sample, normal-resolution FORC diagrams are shown (field spacing between FORCs = 3 mT) above high-resolution FORC diagrams (field spacing between FORCs = 0.7 mT). See text for discussion.

inate among magnetic interactions, superparamagnetic, single-domain, and multidomain grains and to identify individual magnetic components within samples which contain complex mixtures of particles. Further work is necessary to provide an improved understanding of PSD behavior and the manifestations of PSD grains on FORC diagrams. Based on the results presented in this paper, however, it is clear that qualitative interpretation of FORC diagrams provides more information than existing techniques for understanding the magnetic components within natural samples. Development of quantitative tools for interpreting FORC diagrams should improve these capabilities. We are currently developing software, which will be made freely available to interested parties, to enable construction of FORC diagrams using output data from alternating

gradient magnetometers and vibrating sample magnetometers. This should facilitate wider access to FORC diagrams and will enable testing of the interpretive value of FORC diagrams with a far wider range of materials.

Acknowledgments. This work was supported by the University of Southampton Annual Grants Scheme, the Center for Statistics in Science and Technology at the University of California, Davis, and the U.S. National Science Foundation (EAR-9628507 and EAR-9909468). A.P.R. also gratefully acknowledges sabbatical leave support from the Royal Society of London, which enabled preparation of this paper. We are grateful to Joe Stoner, Franz Heider, Mary Kovacheva, Shouyun Hu, Akira Hayashida, Horst-Ulrich Worm, the Ocean Drilling Program, and the Cape Roberts Project for supplying samples. We are also grateful to Tim Rolph, John Dearing, Horst-Ulrich Worm, Mark Dekkers, and Tom Mullender for constructive comments on an earlier version of the manuscript.

References

Bate, G., Statistical stability of the Preisach diagram for particles of γ-Fe_2O_3, *J. Appl. Phys., 33*, 2263-2269, 1962.

Bertotti, G., V. Basso, and A. Magni, Stochastic dynamics in quenched-in disorder and hysteresis, *J. Appl. Phys., 85*, 4355-4357, 1999.

Channell, J. E. T., and C. McCabe, Comparison of magnetic hysteresis parameters of unremagnetized and remagnetized limestones, *J. Geophys. Res., 99*, 4613-4623, 1994.

Chikazumi, S., *Physics of Magnetism*, 554 pp., John Wiley, New York, 1964.

Cisowski, S., Interacting vs. non-interacting single domain behavior in natural and synthetic samples, *Phys. Earth Planet. Inter., 26*, 56-62, 1981.

Corradi, A. R., and E. P. Wohlfarth, Influence of densification on the remanence, the coercivities and the interaction field of elongated γFe_2O_3 powders, *IEEE Trans. Magn., MAG-14*, 861-863, 1978.

Dankers, P., Relationship between median destructive field and remanent coercive forces for dispersed natural magnetite, titanomagnetite and hematite, *Geophys. J. R. Astron. Soc., 64*, 447-461, 1981.

Day, R., M. Fuller, and V. A. Schmidt, Magnetic hysteresis properties of synthetic titanomagnetites, *Phys. Earth Planet. Inter., 13*, 260-266, 1977.

Dekkers, M. J., Magnetic properties of natural goethite, I, Grain-size dependence of some low- and high-field related rock magnetic parameters measured at room temperature, *Geophys. J., 97*, 323-340, 1989.

Dunlop, D. J., Preisach diagrams and remanent properties of interacting monodomain grains, *Philos. Mag., 19*, 369-378, 1969.

Dunlop, D. J., The rock magnetism of fine particles, *Phys. Earth Planet. Inter., 26*, 1-16, 1981.

Dunlop, D. J., and Ö. Özdemir, *Rock Magnetism: Fundamentals and Frontiers*, 573 pp., Cambridge Univ. Press, New York, 1997.

Dunlop, D. J., M. F. Westcott-Lewis, and M. E. Bailey, Preisach diagrams and anhysteresis: Do they measure interactions?, *Phys. Earth Planet. Inter., 65*, 62-77, 1990.

Eick, P. M., and C. M. Schlinger, The use of magnetic susceptibility and its frequency dependence for delineation of a magnetic stratigraphy in ash-flow tuffs, *Geophys. Res. Lett., 17*, 783-786, 1990.

Fabian, K., and T. von Dobeneck, Isothermal magnetization of samples with stable Preisach function: A survey of hysteresis, remanence, and rock magnetic parameters, *J. Geophys. Res., 102*, 17,659-17,677, 1997.

Flanders, P. J., A vertical force alternating-gradient magntometer, *Rev. Sci. Instrum., 61*, 839-847, 1990.

Girke, H., Der Einfluß innerer magnetischer Kopplungen auf die Gestalt der Preisach-Funktionen hochpermeabler Materialen, *Z. Angew. Phys., 11*, 502-508, 1960.

Hayashida, A., H. Kamata, and T. Danhara, Correlation of widespread tephra deposits based on paleomagnetic directions: Link between a volcanic field and sedimentary sequences in Japan, *Quat. Int., 34-36*, 89-98, 1996.

Heider, F., U. Körner, and P. Bitschene, Volcanic ash particles as carriers of remanent magnetization in deep-sea sediments from the Kerguelen Plateau, *Earth Planet. Sci. Lett., 118*, 121-134, 1993.

Hejda, P., and T. Zelinka, Modelling of hysteresis processes in magnetic rock samples using the Preisach diagram, *Phys. Earth Planet. Inter., 63*, 32-40, 1990.

Hejda, P., E. Petrovsky, and T. Zelinka, The Preisach diagram, Wohlfarth's remanence formula and magnetic interactions, *IEEE Trans. Magn., MAG-30*, 896-898, 1994.

Ivanov, V. A., and L. Y. Sholpo, Quantitative criteria for single- and multi-domain states in ferromagnetic minerals in rocks, *Izv. Earth Phys., 18*, 612-616, 1982.

Ivanov, V. A., I. A. Khaburzaniya, and L. Y. Sholpo, Use of Preisach diagram for diagnosis of single- and multi-domain grains in rock samples, *Izv. Earth Phys., 17*, 36-43, 1981.

Jackson, M., Diagenetic sources of stable remanence in remagnetized Paleozoic cratonic carbonates: A rock magnetic study, *J. Geophys. Res., 95*, 2753-2761, 1990.

Kovacheva, M., Archaeomagnetic database from Bulgaria: The last 8000 years, *Phys. Earth Planet. Inter., 102*, 145-151, 1997.

Lehman, B., C. Laj, C. Kissel, A. Mazaud, M. Paterne, and L. Labeyrie, Relative changes of the geomagnetic field intensity during the last 280 kyear from piston cores in the Açores area, *Phys. Earth Planet. Inter., 93*, 269-284, 1996.

Mayergoyz, I. D., Mathematical models of hysteresis, *IEEE Trans. Magn., MAG-22*, 603-608, 1986.

McCabe, C., and J. E. T. Channell, Late Paleozoic remagnetization in limestones of the Craven Basin (northern England) and the rock magnetic fingerprint of remagnetized sedimentary carbonates, *J. Geophys. Res., 99*, 4603-4612, 1994.

Mehra, O. P., and M. L. Jackson, Iron oxide removal from soils and clays by a dithionite-citrate system buffered with sodium bicarbonate, *Clays Clay Miner., 5*, 317-327, 1960.

Mullins, C. E., and M. S. Tite, Preisach diagrams and magnetic viscosity phenomena for soils and synthetic assemblies of iron oxide grains, *J. Geomagn. Geoelectr., 25*, 213-229, 1973.

Néel, L., Remarques sur la théorie des propriétés magnétiques des substances dures, *Appl. Sci. Res., Sect. B, 4*, 13-24, 1954.

Néel, L., Some theoretical aspects of rock magnetism, *Adv. Phys., 4*, 191-243, 1955.

Parry, L. G., Magnetization of immobilized particle dispersions with two distinct particle sizes, *Phys. Earth Planet. Inter., 28*, 230-241, 1982.

Pike, C. R., A. P. Roberts, and K. L. Verosub, Characterizing interactions in fine magnetic particle systems using first order reversal curves, *J. Appl. Phys., 85*, 6660-6667, 1999.

Pike, C. R., A. P. Roberts, and K. L. Verosub, FORC diagrams and thermal relaxation effects in magnetic particles, *Geophys. J. Int.*, in press, 2000.

Preisach, F., Über die magnetische Nachwirkung, *Z. Phys., 94*, 277-302, 1935.

Roberts, A. P., Magnetic properties of sedimentary greigite (Fe_3S_4), *Earth Planet. Sci. Lett., 134*, 227-236, 1995.

Roberts, A. P., K. L. Verosub, R. J. Weeks, B. Lehman, and C. Laj, Mineral magnetic properties of Middle and Late Pleistocene sediments at ODP sites 883, 884 & 887, North Pacific Ocean, *Proc. Ocean Drill. Program, Sci. Results, 145*, 483-490, 1995a.

Roberts, A. P., Y. L. Cui, and K. L. Verosub, Wasp-waisted hysteresis loops: Mineral magnetic characteristics and discrimination of components in mixed magnetic systems, *J. Geophys. Res., 100*, 17,909-17,924, 1995b.

Roberts, A. P., R. L. Reynolds, K. L. Verosub, and D. P. Adam, Environmental magnetic implications of greigite (Fe_3S_4) formation in a 3 million year lake sediment record from Butte Valley, northern California, *Geophys. Res. Lett., 23*, 2859-2862, 1996.

Roberts, A. P., G. S. Wilson, F. Florindo, L. Sagnotti, K. L. Verosub, and D. M. Harwood, Magnetostratigraphy of lower Miocene strata from the CRP-1 core, McMurdo Sound, Ross Sea, Antarctica, *Terra Antart., 5*, 443-453, 1998.

Schlinger, C. M., J. G. Rosenbaum, and D. R. Veblen, Fe-oxide microcrystals in welded tuff from southern Nevada: Origin of remanence carriers by precipitation in volcanic glass, *Geology, 16*, 556-559, 1988.

Smith, R. T., and K. L. Verosub, Thermoviscous remanent magnetism of Columbia River Basalt blocks in the Cascade landslide, *Geophys. Res. Lett., 21*, 2661-2664, 1994.

Sprowl, D. R., Numerical estimation of interactive effects in single-domain magnetite, *Geophys. Res. Lett., 17*, 2009-2012, 1990.

Stoner, J. S., J. E. T. Channell, and C. Hillaire-Marcel, The magnetic signature of rapidly deposited detrital layers from the deep Labrador Sea: Relationship to North Atlantic Heinrich layers, *Paleoceanography, 11*, 309-325, 1996.

Tarduno, J. A., Temporal trends of magnetic dissolution in the pelagic realm: Gauging paleoproductivity?, *Earth Planet. Sci. Lett., 123*, 39-48, 1994.

Tauxe, L., Sedimentary records of relative paleointensity of the geomagnetic field: Theory and practice; *Rev. Geophys., 31*, 319-354, 1993.

Tauxe, L., T. A. T. Mullender, and T. Pick, Potbellies, wasp-waists, and superparamagnetism in magnetic hysteresis, *J. Geophys. Res., 101*, 571-583, 1996.

Vajda, F., and E. Della Torre, Relationship between the moving and the product Preisach model, *IEEE Trans. Magn., MAG-27*, 3823-3826, 1991.

Verosub, K. L., P. Fine, M. J. Singer, and J. TenPas, Pedogenesis and paleoclimate: Interpretation of the magnetic susceptibility record of Chinese loess-paleosol sequences, *Geology, 21*, 1011-1014, 1993.

Wang, S. M., S. Y. Hu, E. Appel, X. H. Ma, V. Hoffmann, Z.M. Sun, X. D. Yang, Y. Ma, and H. X. Pan, Incursion of sea water into Gucheng Lake detected by magnetic, biologic and chemical data, *Phys. Chem. Earth, A24*, 805-810, 1999.

Wasilewski, P., Magnetic hysteresis in natural materials, *Earth Planet. Sci. Lett., 20*, 67-72, 1973.

Worm, H.-U., On the superparamagnetic-stable single domain transition for magnetite and frequency dependence of susceptibility, *Geophys. J. Int., 133*, 201-206, 1998.

Worm, H.-U., Time-dependent IRM: A new technique for magnetic granulometry, *Geophys. Res. Lett., 26*, 2557-2560, 1999.

Worm, H.-U., and M. Jackson, The superparamagnetism of Yucca Mountain Tuff, *J. Geophys. Res., 104*, 25,415-25,425, 1999.

Xu, S., and D. J. Dunlop, Theory of partial thermoremanent magnetization in multidomain grains 2. Effect of microcoercivity distribution and comparison with experiment, *J. Geophys. Res., 99*, 9025-9033, 1994.

Zelinka, T., P. Hejda, and V. Kropacek, The vibrating-sample magnetometer and Preisach diagram, *Phys. Earth Planet. Inter., 46*, 241-246, 1987.

C. R. Pike and K.L. Verosub, Department of Geology, University of California, Davis, CA 95616.

A. P. Roberts, School of Ocean and Earth Science, University of Southampton, Southampton Oceanography Centre, European Way, Southampton SO14 3ZH, England, UK. (arob@mail.soc.soton.ac.uk).

(Received April 12, 2000; revised July 16, 2000;
accepted August 30, 2000.)